AGU PUBLICATIONS

Journal of Advances in Modeling Earth Systems

RESEARCH ARTICLE
10.1002/2015MS000481

Poleward migration of eddy-driven jets

R. Chemke[1] and Y. Kaspi[1]

[1]Department of Earth and Planetary Sciences, Weizmann Institute of Science, Rehovot, Israel

Key Points:
- Eddy driven jets migrate poleward with time
- The planet's sphericity causes a poleward biased baroclinicity and eddy momentum flux convergence
- At high rotation rates as narrower jets form the migration rate decreases

Supporting Information:
- Supporting Information S1
- Supporting Information S2

Correspondence to:
R. Chemke,
rei.chemke@weizmann.ac.il

Citation:
Chemke, R., and Y. Kaspi (2015), Poleward migration of eddy-driven jets, *J. Adv. Model. Earth Syst.*, *07*, doi:10.1002/2015MS000481.

Received 5 MAY 2015
Accepted 21 AUG 2015
Accepted article online 26 AUG 2015

Abstract Poleward migration of eddy-driven jets is found to occur in the extratropics when the subtropical and eddy-driven jets are clearly separated, as achieved by simulations at high-rotation rates. The poleward migration of these eddy-driven baroclinic jets over time is consistent with variation of eddy momentum flux convergence and baroclinicity across the width of the jet. We demonstrate this using a high-resolution idealized GCM where we systematically examine the eddy-driven jets over a wide range of rotation rates (up to 16 times the rotation rate of Earth). At the flanks of the jets, the poleward migration is caused by a poleward bias in baroclinicity across the width of the jet, estimated through measures such as Eady growth rate and supercriticality. The poleward biased baroclinicity is due to the meridional variation of the Coriolis parameter, which causes a poleward bias of the eddy momentum flux convergence. At the core of the jets, the poleward biased eddy momentum flux convergence relative to the mean jet deflects over time the baroclinicity and the jets poleward. As the rotation rate is increased, and more (narrower) jets emerge the migration rate becomes smaller due to less eddy momentum flux convergence over the narrower baroclinic zones. We find a linear relation between the migration rate of the jets and the net eddy momentum flux convergence across the jets. This poleward migration might be related to the slow poleward propagation of temporal anomalies of zonal winds observed in the upper troposphere.

1. Introduction

Atmospheric jets play a key role in shaping the Earth's climate through eddy-mean flow interactions. The latitudinal location of the jets in the extratropics has a large effect on weather and storm track variability [*Blackmon*, 1976; *Blackmon et al.*, 1977]. There are observations dating back to the 1950s that anomalies of the zonal jets propagate poleward with time [*Riehl et al.*, 1950]. *Dickey et al.* [1992] suggested that such long time scale poleward momentum propagation is related to the occurrence of El Niño and La Niña events. *Feldstein* [1998] showed using reanalysis data that poleward migration of zonal-mean relative angular momentum anomalies occurs at high (low) latitudes due to low (high) frequency transient eddy momentum flux convergence feedback. In addition, *James et al.* [1994] used a simplified GCM to capture the low frequency of the zonal wind. They showed that the zonal wind zonal mean anomalies migrate poleward at a rate of one degree latitude per day in a reoccurring sequence every 60–70 days. The time scale of this propagation (40–60 days) [*Riehl et al.*, 1950; *Feldstein*, 1998] is relatively long compared to the variations in the radiation intensity associated with the seasonality on Earth, and therefore observations of this phenomenon are difficult.

Nonetheless, due to the importance of understanding zonal jet behavior and their implications on global and regional climate, several studies have attempted to provide a mechanism for this phenomenon. *James and Dodd* [1996] showed that the meridional wave number of the equatorward propagating Rossby wave causes a poleward bias in the eddy momentum flux convergence around the jet's core. As a result, the zonal wind migrates poleward toward the wave's origin at a velocity of 0–2 m s^{-1}. *Robinson* [2000] argued that due to the sphericity of the planet, the asymmetry of the meridional wave propagation [e.g., *Held and Hoskins*, 1985; *Whitaker and Snyder*, 1993] causes the convergence of the EP flux to occur equatorward of the generation latitude of the eddies. This produces a residual circulation, which reinforces the baroclinicity at lower levels, poleward of the generation latitude of the eddies. Thus, the eddies push the baroclinicity poleward. *Lee et al.* [2007] showed that the homogenization of PV through Rossby wave breaking halts the propagation of these waves equatorward. As the critical latitude migrates poleward, so do the negative and positive zonal wind anomalies. The reconstruction of the westerlies through temperature relaxation, enables the Rossby waves to reinvade lower latitudes. Other studies [*Lorenz*, 2014a,b] have also discussed the importance of the critical and reflective levels in shifting the zonal wind anomalies poleward.

Similar jet migration, though equatorward, has been seen in ocean models as well. *Chan et al*. [2007] showed using a semihemisphere zonally reentrant ocean model that the secondary jets from the equator in the ocean form at high latitudes, and slowly migrate equatorward. Their proposed mechanism relies on the fact that around each secondary jet in their model, the static stability increases equatorward; hence, the Eady growth rate develops an asymmetry around the zonal axis of the eddy-driven jet. This in turn, causes an asymmetry in the eddy heat fluxes around the zonal axes of the jet, which produce a residual meridional velocity. Due to mass conservation a residual circulation will form, which will cool the core of the jet, thus, moving the maximum baroclinic zone away toward latitudes with higher values of static stability (equatorward). Similar equatorward migration of off-equatorial barotropic oceanic jets was found in a model of an ice covered ocean (Y. Ashkenazy and E. Tziperman, Variability, instabilities and eddies in a Snowball ocean, submitted to *Journal of Climate*, 2015).

From an eddy life cycle point of view, *Orlanski* [2003] showed that anticyclonic (cyclonic) wave breaking due to the β effect causes a westerly (easterly) flow at the poleward side of the eddy axis. Following on this, *Riviere* [2009] showed, using the Rossby waves refractive index, that there is a poleward displacement of the upper layer jet due to the absolute vorticity component in the gradient of the potential vorticity, which favors anticyclonic wave breaking. In addition, due to the β effect, there is a positive eddy feedback that will cause the jet to propagate poleward. Such poleward propagation is particularly evident downstream of the Atlantic and Pacific storm track entrance regions [*Chang et al*., 2002].

On Earth, due to the relatively large typical eddy length scale compared to the size of the planet, the eddy-driven jet usually is partially merged with the subtropical jet and captures a significant part of the baroclinic zone. As a result, and due to the seasonal variations, it is difficult to identify any mechanism of poleward migration, resulting in both previous observational and modeling studies using various filtering methods in order to identify these migrating anomalies [e.g., *Feldstein*, 1998; *Lee et al*., 2007]. Here, in order to isolate only the eddy-driven jets and to examine multiple jet regimes (where jet migration is more pronounced), we study a series of simulations where we vary the rotation rate of the planet. This allows both separating the eddy-driven jet from the subtropical jet, and studying the dependence of the poleward migration on the rotation rate of the planet, which turns out to be important for understanding the poleward migration. Planets with higher rotation rates exhibit multiple zonal jets due to eddy length scales becoming smaller as rotation rate is increased [*Williams and Holloway*, 1982; *Vallis and Maltrud*, 1993; *Cho and Polvani*, 1996; *Navarra and Boccaletti*, 2002; *Kaspi and Schneider*, 2011, *Kaspi and showman*, 2015; *Chemke and Kaspi*, 2015]. Concomitantly, as the rotation rate of a planet is increased, the Hadley cell becomes narrower and less intense, resulting in more equatorward and weaker subtropical jets [e.g., *Held and Hou*, 1980; *Walker and Schneider*, 2006]. Purely eddy-driven jets, which are distinct from the subtropical jets, form in our simulations only at rotation rates faster than Earth's rotation rate.

In this study, we use the variation of rotation rate as a method of varying the eddy length scale. Alternatively, we could have varied the planetary radius or thermal Rossby number [e.g., *Mitchell and Vallis*, 2010], but for demonstrating the jet migration we find that varying only the rotation rate captures this mechanism most clearly. Experimenting with fast rotation rates and thus a regime of multi-eddy-driven jets, enables the quantitative study of the poleward migration of these jets.

Section 2 describes briefly the idealized GCM and analysis methods. The jet migration in our simulations, and the proposed mechanism for the poleward propagation are presented in sections 3 and 4, respectively. Section 5 demonstrates the properties of the poleward migration over multiple eddy length scales, jet widths, and migration rates by varying the planetary rotation rate. The results are further discussed in section 6.

2. Model

We use an idealized aquaplanet moist global circulation model (GCM), based on the GFDL flexible modeling system (FMS). This is a 3-D spherical coordinate primitive equation model of an ideal-gas atmosphere set at perpetual equinox similar to *Frierson et al*. [2006] and *O'Gorman and Schneider* [2008a]. The lower boundary of the model is an ocean slab with no topography. The model does not contain a representation for ocean dynamics (heat transport, etc.), thus, the surface temperature only changes due to heat transport between the ocean slab and the lower layer of the atmosphere through radiative, sensible, and latent heat fluxes.

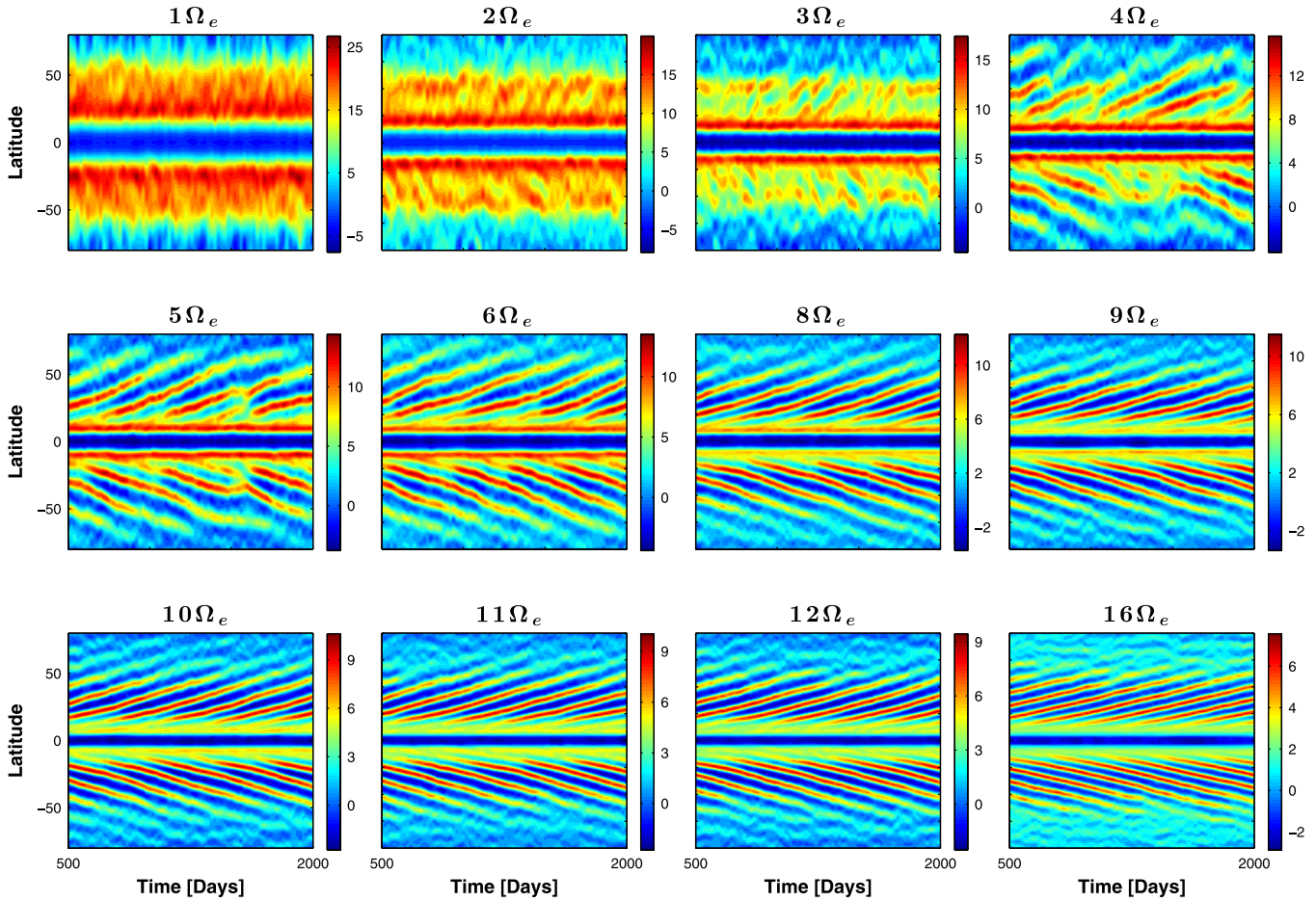

Figure 1. Hovmoller diagrams of zonal and vertical averaged zonal wind ($\bar{u}$, m s^{-1}) as a function of time for different simulations at rotation rates between Ω_e and $16\Omega_e$. Note the different color scales for each plot.

The parameterization of the surface fluxes (sensible heat, latent heat, and water vapor) and the boundary layer is based on the Monin-Obukhov similarity theory. The model contains a constant latitudinal distribution of solar radiation at the top of the atmosphere and a standard two-stream gray radiation scheme for long-wave radiation [*Held*, 1982], with optical depths that are only a function of latitude and pressure [*Frierson et al.*, 2006].

We carry out a set of experiments where we systematically increase the planetary rotation rate up to 16 times Earth's rotation rate (Ω_e). Each simulation has 30 vertical sigma layers at T170 horizontal resolution (0.7° × 0.7°). Simulation results presented here have a 6 h temporal resolution (model time step is 150 s), and have been zonally and vertically averaged, in addition to a running time average of 20 days. The atmosphere reaches a periodic jet migration state by day 200, and the results represent the last 1500 days of 2000 day runs. The periodic jet migration state in these simulations is a state where the eddy-driven jets are constantly forming near the subtropical jet and migrating poleward. Thus, the simulation results we present are not at steady state.

3. Jet Migration

In this section, we present a set of simulations with rotation rates faster than Earth's (hence smaller eddy length scales), where the eddy-driven jets and their poleward migration can be clearly identified. We begin with demonstrating the jet migration over a series of simulations, and then proceed to explain the migration mechanism. Figure 1 shows Hovmoller diagrams, from simulations at different rotation rates, of the zonal and vertical averaged zonal wind, $\overline{u}$. Four interesting properties can be seen in this plot: First, a clear

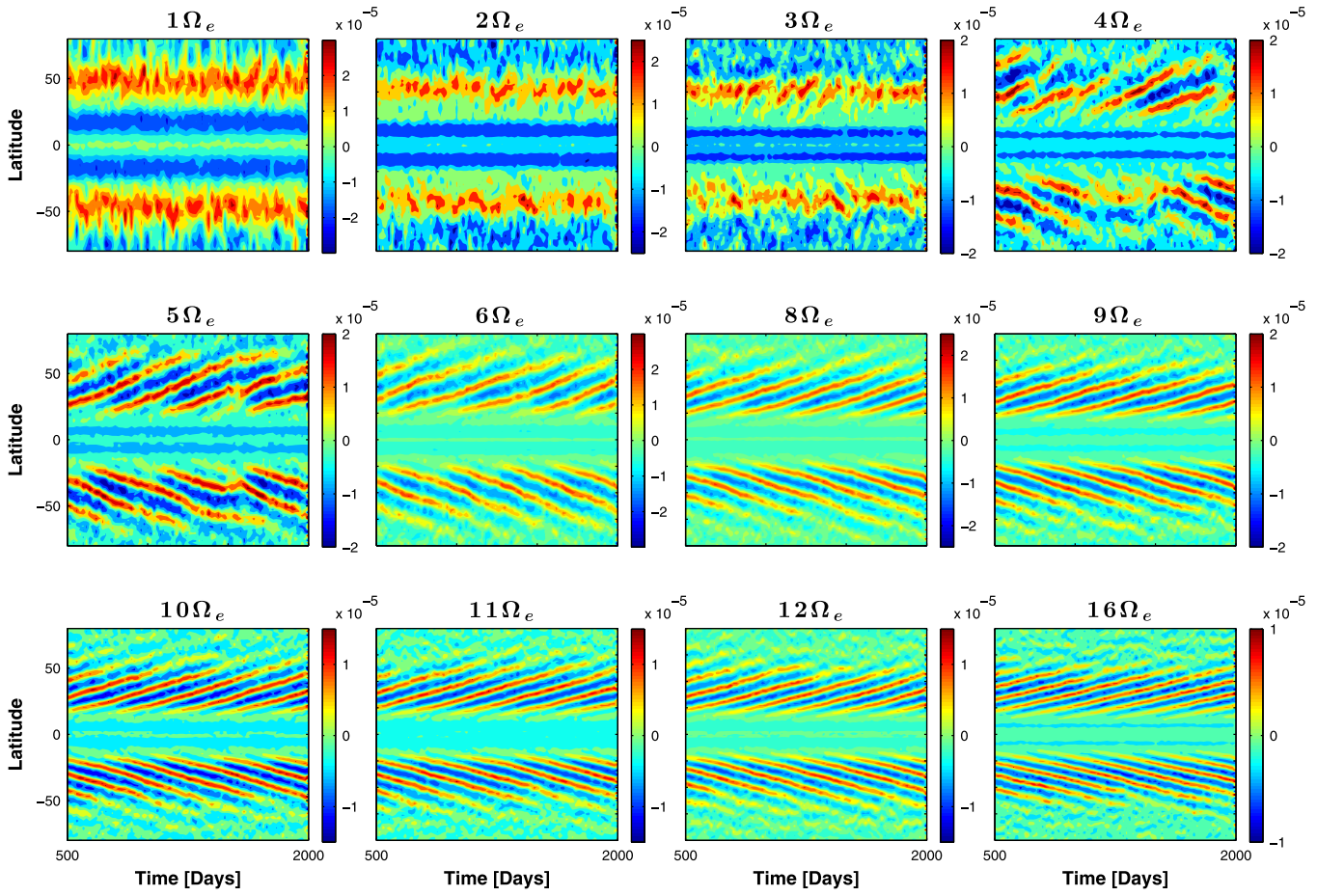

Figure 2. Hovmoller diagrams of zonal and vertical averaged eddy momentum flux convergence (N_y, m s^{-2}) as a function of time for different simulations at rotation rates between Ω_e and $16\Omega_e$. Note the different color scales for each plot.

separation between the eddy-driven jet and the subtropical jet begins at rotation rates faster than $2\Omega_e$. Different than the observations and previous modeling studies where the migration referred to the zonal wind anomalies [*Riehl et al.*, 1950; *Dickey et al.*, 1992; *Feldstein*, 1998; *Lee et al.*, 2007; *Chan et al.*, 2007], here the poleward migration of the eddy-driven jets themselves is clear. Second, the subtropical jet does not change its latitudinal location with time, and is determined by the latitudinal extent of the Hadley cell, which moves equatorward with increasing rotation rate [*Held and Hou*, 1980; *Walker and Schneider*, 2006; *Kaspi and Showman*, 2015]. Third, the number of jets, as in *Williams and Holloway* [1982], shows an increase with rotation rate; and fourth, the rate of poleward migration of the eddy-driven jets decreases with rotation rate. These last two points are discussed in detail in section 5. Furthermore, as pointed out by *Son and Lee* [2006] in the context of zonal wind anomalies, the continuous migration of the eddy-driven jet is different from the phenomenon of jet meandering (zonal index) [e.g., *Robinson*, 2000], or from the jet's meridional shift due to external forcing in a steady state [e.g., *Kidston et al.*, 2011; *Barnes and Thompson*, 2014; *Lorenz*, 2014a,b; *Zurita-Gotor et al.*, 2014].

The vertically integrated zonal momentum QG equation to leading order is given by

$$\frac{\partial \overline{u}}{\partial t} = -\frac{1}{a\cos^2\theta}\frac{\partial(\overline{u'v'}\cos^2\theta)}{\partial\theta} + F, \tag{1}$$

where primes denote deviation from the zonal mean (overbars), a is Earth's radius, θ is latitude, v is meridional velocity, and F represents surface drag. This shows how the eddy momentum flux convergence can accelerate or decelerate the jet [*Vallis*, 2006]. As a result of the vertical integration, the Coriolis term ($f\overline{v}$) in the QG

momentum equation vanishes due to mass conservation. In addition, mainly due to the zonal average, the mean momentum flux convergence terms are small compared to the eddy momentum flux convergence terms. Figure 2 shows Hovmoller diagrams similar to those in Figure 1 only for the zonal mean eddy momentum flux convergence, N_y (following the notation of *Hoskins et al.* [1983], and in spherical coordinates),

$$N_y \equiv -\frac{1}{a\cos^2\theta}\frac{\partial(\overline{u'v'}\cos^2\theta)}{\partial\theta}. \quad (2)$$

The eddy momentum flux convergence shows the same signature of migration as the jets themselves, and the correlation between the momentum flux convergence regions (Figure 2) and the extratropical jets (Figure 1) indicates that indeed these jets are eddy driven. The lack of momentum flux convergence at the location of the equatormost and nonmigrating jet, indicates that this is a subtropical jet, located at the edge of the Hadley cell. Only for the lowest rotation rate cases this separation between the subtropical and eddy-driven jet is not distinct.

4. Jet Migration Mechanism

Carrying on the results of the previous section, here, we propose a mechanism for the poleward migration of the eddy-driven jets, by focusing first on one simulation with a rotation rate of $8\Omega_e$. In the next section, we show the consistency of this mechanism for all other rotation rates we explored, in addition to the rotation rate's effect on the jet migration rate.

Figure 3 shows a latitudinal cross section of $\bar{u}$ and N_y for a specific time of this simulation. It shows the latitudinal correlation in each eddy-driven jet between $\bar{u}$ and N_y, and the lower values of N_y at the latitudes of the subtropical jets. Moreover, N_y has a poleward bias around each eddy-driven jet. In order to demonstrate this poleward bias more clearly, and to show how robust this bias is for all the eddy-driven jets through the entire simulation, we sum N_y (ΣN_y) separately over the poleward and equatorward flanks of each eddy-driven jet, and plot ΣN_y over the poleward flank ($\Sigma_p N_y$) versus ΣN_y over the equatorward flank ($\Sigma_e N_y$) for each jet (Figure 4). The meridional width of each flank is defined as the distance between the latitude of maximum vertically averaged mean zonal wind within each jet, and its closest latitude of minimum or zero zonal wind. Summing over the full latitudinal width of the jet flanks, and not comparing only the closest poleward and equatorward points around the jet's peak enables accumulating better statistics for each jet, and thus accounting the total effect that the eddy momentum flux convergence has on the whole jet and not only on its peak. This also accounts for the meridional structure of both the eddy-driven jet and eddy momentum flux convergence. In addition, it accounts for the migration of the jet even in cases where the peak of the jet (represented by a single point) has not moved meridionally or moved in a different direction. Each dot in Figure 4 represents an eddy-driven jet at a specific time and latitude. The black line represents the line where $\Sigma_p N_y$ equals $\Sigma_e N_y$ for a given jet (i.e., a slope of unity in this plot). A jet (dot) for which its $\Sigma_p N_y$ is larger than its $\Sigma_e N_y$, appears therefore above the black line, and vice verse. In Figure 4, 88% of the jets experience a larger poleward bias in ΣN_y (placed above the black line). This means that statistically most of the jets through the 1500 days of this model run ($8\Omega_e$), experience a poleward bias in ΣN_y.

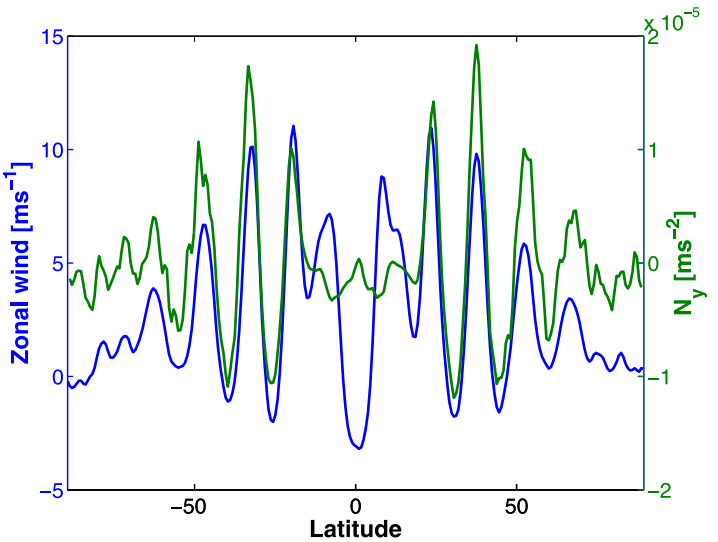

Figure 3. Vertical and zonal mean zonal wind ($\bar{u}$, blue), and eddy momentum flux convergence (N_y, green) as a function of latitude for a specific time in the $8\Omega_e$ simulation. Results are smoothed with a 20 day running mean.

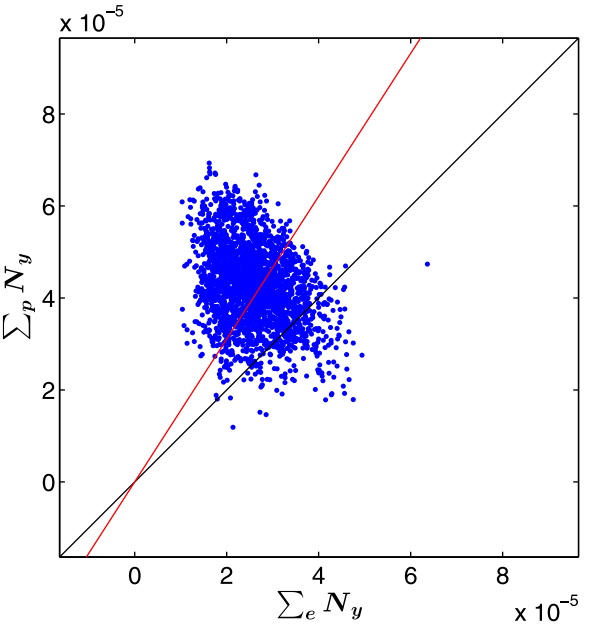

Figure 4. The sum over the poleward (Σ_p) versus equatorward (Σ_e) flanks of the eddy momentum flux convergence (N_y, m s^{-2}) for all jets in the 8 Ω_e simulation. Each dot represents a jet at a certain time and latitude. The black line represents a line where the sum of the eddy momentum flux convergence over the poleward flank ($\sum_p N_y$) is equal to the sum of the eddy momentum flux convergence over the equatorward flank ($\Sigma_e N_y$). The red line represents the best fit for the data based on a linear regression analysis.

In order to quantify the magnitude of this poleward bias, we perform a linear regression analysis (red line) on the data presented in Figure 4. When the slope of this line equals that of the black line (1:1), the mean magnitude of the poleward bias equals to that of the equatorward bias. In Figure 4, the slope of this line is about 1.55, which means that most of the jets experience a strong poleward bias of ΣN_y. Therefore, over most instances of the simulation time, the momentum flux convergence in equation (1) is stronger on the poleward flank of the jets, and therefore supports a poleward migration of the jets. Similarly, previous studies have also shown the importance of eddy momentum flux convergence in propagating the mean zonal wind anomalies [e.g., *Feldstein*, 1998; *Lee et al*., 2007; *James and Dodd*, 1996], as expected from equation (1).

The group velocity of Rossby waves propagates away from the source region. Therefore, in the presence of Rossby waves there is an eddy momentum flux convergence at the source region (in our case, the baroclinic unstable region) [*Vallis*, 2006]. Using a QG model, *Riviere* [2009] showed that the waves with the largest growth rates are dominant in shifting the jet poleward. Hence, an increase in baroclinic growth can enhance poleward propagation of the jet. Thus, we next analyze the meridional location of baroclinicity (eddy generation) in order to study its location relative to the eddy momentum flux convergence and the eddy-driven jet.

As the simplest possible baroclinicity measure, we first use the Eady growth rate, σ, [*Eady*, 1949; *Pedlosky*, 1987] which represents the growth rate of the most unstable waves as a simple local measure for the baroclinicity [e.g., *Stone*, 1966; *Ioannou and Lindzen*, 1986; *Hoskins and Valdes*, 1990; *Lorenz and Hartmann*, 2001; *Chan et al*., 2007; *Smith*, 2007; *Merlis and Schneider*, 2009],

$$\sigma = \frac{fU_z}{S}, \tag{3}$$

where f is the Coriolis parameter, U_z is the vertical shear of the zonal wind, and $S = \left(\frac{g}{\bar{\theta}}\frac{\partial \bar{\theta}}{\partial z}\right)^{1/2}$ is the static stability. Despite the fact that the Eady growth rate was developed on the f-plane, *Lindzen and Farrell* [1980] showed that the Eady growth rate is also suitable to represent the growth rate of the most unstable waves on a beta plane as in Charney's model [*Charney*, 1947]. Nonetheless, we will later investigate the jet migration mechanism with other measures of baroclinicity such as the supercriticality parameter [e.g., *Held and Larichev*, 1996]. Figure 5a shows the sum over the poleward and equatorward flanks, defined as for the momentum flux convergence in Figure 4, but for the zonally and vertically averaged Eady growth rate. As for N_y, the Eady growth rate also shows a clear poleward bias around the jet's core. About 83% of the jets experience a poleward bias in the Eady growth rate, with a 1.18 larger magnitude than the equatorward bias (red line).

To better understand why the Eady growth rate has a robust poleward bias around the jet's core, we implement the same analysis on all three components of the Eady growth rate: U_z, S, and f (Figures 6a–6c, respectively). As for the Eady growth rate itself, we look at the vertical average of all three components. The vertical shear of the zonal wind (Figure 6a) is symmetric around the jet's core: only 55% of the jets

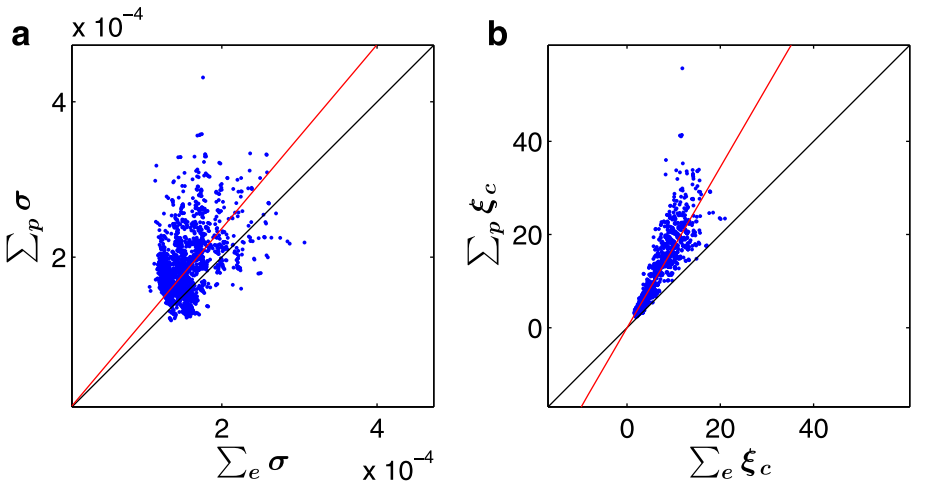

Figure 5. The sum over the poleward (Σ_p) versus equatorward (Σ_e) flanks of (a) the Eady growth rate, σ, s^{-1} and (b) the supercriticality parameter, ξ_c for all jets in the $8\Omega_e$ run. Each dot represents a jet at a certain time and latitude. In each plot, the black line represents a line where the sum over the poleward flank is equal to the sum over the equatorward flank. The red line represents the best fit for the data based on a linear regression analysis.

experience a poleward bias in U_z with approximately the same magnitude as the equatorward bias (only 0.97 larger). Thus, U_z does not contribute to the above poleward bias in the Eady growth rate.

As discussed in section 1, *Chan et al*. [2007] showed that the meridional change of the static stability in the ocean can have a profound effect on the direction of the eddy-driven jet's migration. In the atmosphere, the vertically integrated static stability generally increases poleward. Thus, it can cause an equatorward bias in the Eady growth rate. However, as can be seen in Figure 6b, the static stability is also symmetric around the jet's core; only about 52% of the jets experience a poleward bias in static stability, with approximately the same magnitude as the equatorward bias, which is only 1.07 times larger. Hence, relative to its magnitude, the static stability does not vary much with latitude, and also does not contribute to the poleward bias in the Eady growth rate.

The Coriolis parameter, however, has a clear poleward bias (Figure 6c) as expected from its latitudinal dependence. 91.41% of the jets experience a poleward bias with a 1.26 times larger magnitude than the equatorward bias. In fact, since f is a trigonometric function, we expect that all the jets should experience a poleward bias in f. However, some of the jets (8.59%) experience an equatorward bias in the Coriolis parameter measure. This occurs since the structure of the jets is not always meridionally symmetric (Figure 6a). This asymmetry results in a wider equatorward flank than a poleward flank for some jets. Thus, in a small subset of the cases, the summed Coriolis parameter is larger on the equatorward flank of these jets, even though the value of f always increases poleward. Despite this asymmetry in some of the cases, statistically, the meridional structure of the jets is symmetric around the jet core (Figure 6a). Repeating this analysis of the poleward bias without accounting for the meridional structure of the jets (e.g., by summing over the same amount of latitudes poleward and equatorward of the jet's core) produces the same behavior in all of the above components.

Therefore, the poleward bias of the Eady growth rate around the jet's core is primarily due to the sphericity of the planet (the latitudinal increase of the Coriolis parameter). Since the Eady growth rate was derived from a f-plane theory, and in order to account for the sphericity of the planet (the β-effect in QG), we also examine the supercriticality, ξ_c, as a measure for baroclinicity,

$$\xi_c = \frac{f^2 U_z}{\beta H S^2}, \tag{4}$$

which was found to be suitable for two layer models [*Phillips*, 1954; *Held and Larichev*, 1996], continually stratified models [*Charney*, 1947] and GCMs [*Schneider and Walker*, 2008], where $\beta = \frac{\partial f}{\partial y}$ and H is the tropopause height. Figure 5b shows the same type of analysis as in Figure 5a but for the supercriticality parameter. The height of the tropopause is calculated as the height where the static stability reaches a threshold

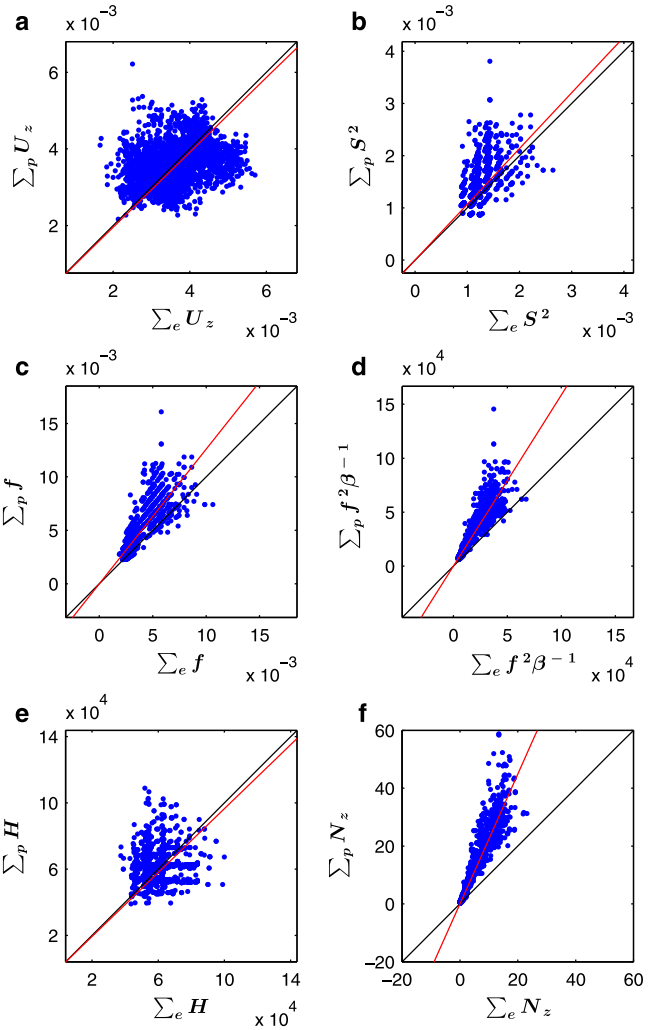

Figure 6. The sum over the poleward (Σ_p) versus equatorward (Σ_e) flanks of (a) the vertical shear of the zonal wind, U_z (s^{-1}); (b) the static stability, S^2 (s^{-2}); (c) the Coriolis parameter, f (s^{-1}); (d) $f^2\beta^{-1}$ ($m\,s^{-1}$); (e) the tropopause height, H (m); (f) the sum of the divergence of the vertical component of the EP flux for all jets in the $8\Omega_e$ run. Each dot represents a jet at a certain time and latitude. In each plot, the black line represents a line where the sum over the poleward flank is equal to the sum over the equatorward flank. The red line represents the best fit for the data based on a linear regression analysis.

value of 0.015 s^{-1} and is symmetric around the jet's core (Figure 6e). The supercriticality has a robust poleward bias around the jet core; about 99% of the jets experience a poleward bias with a 1.72 larger magnitude than the equatorward bias. As in the Eady growth rate case, the main contributors to the poleward bias in supercriticality is its Coriolis related parameter, $f^2\beta^{-1}$ (Figure 6d).

The eddy-mean flow energy cycle describes the conversion of mean available potential energy to mean kinetic energy through eddy heat and momentum fluxes [*Lorenz*, 1955]. *Simmons and Hoskins* [1978] showed that the perturbation life cycle plays an important role in this cycle. As the perturbation grows through baroclinic instability while subtracting potential energy from the mean flow, it eventually decays barotropically and returns kinetic energy to the mean flow by eddy momentum fluxes. In our simulations, in addition to the poleward biased eddy momentum flux convergence, the divergence of the vertical component of the EP flux, following *Edmon et al.* [1980], also has a poleward bias around the jet's core (Figure 6f). About 82% of the jets experience a poleward bias in the divergence of the vertical component of the EP flux, with a 2.25 larger magnitude than the equatorward bias (red line).

To examine the causality between the mean zonal wind, Eady growth rate, and eddy momentum flux convergence, we produce a composite of these fields at all latitudes and times (blue, red, and green lines in Figure 7, respectively). The reference time for this composition (lag 0 in Figure 7) is the minimum in the Eady growth rate around each cycle (between two consecutive maxima of the mean zonal wind). Choosing a different reference time (e.g., the minimum or maximum of the mean zonal wind) produces the same results. For ease of comparison, the Eady growth rate and eddy momentum flux convergence were rescaled using a linear regression analysis with the mean zonal wind. Around each peak of the mean zonal wind (blue line, Figure 7), the left branch is what we referred to as the poleward flank in Figure 3 (since when looking from a specific latitude the poleward flank appears prior to the arrival of the peak). At the flanks of the jets (i.e., at times between 0 and 100 days and after 250 days) the Eady growth rate precedes the eddy momentum flux convergence that precedes the mean zonal wind. However, around the jet's core (i.e., at times between 100 and 250 days), the eddy momentum flux convergence precedes the Eady growth rate, which precedes the mean zonal wind.

At the flanks of the jet, the vertical shear of the zonal wind is weak, and thus the poleward bias in the Coriolis parameter causes the poleward bias in baroclinicity, which results in the bias of the eddy momentum flux convergence. Around the jet's core, on the other hand, the baroclinicity is more affected by the strong

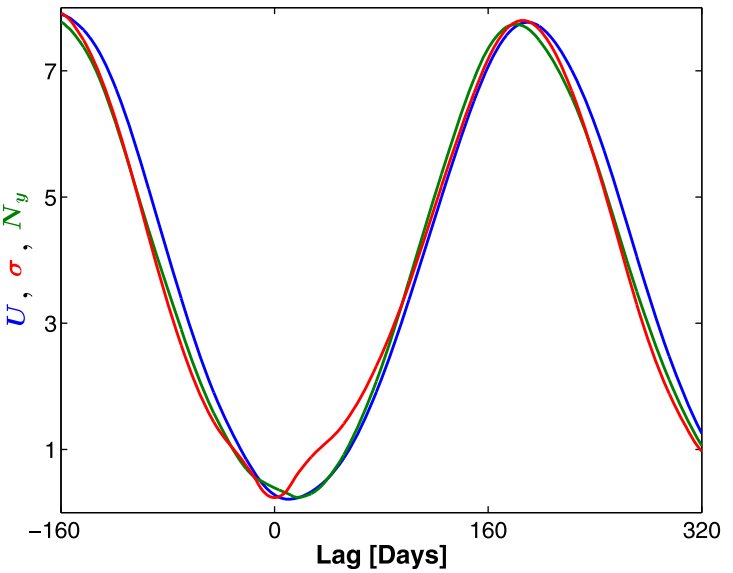

Figure 7. The composite time series over all latitudes of the mean zonal wind (blue), m s^{-1}, Eady growth rate (red), 10^{-5} s^{-1}, and the eddy momentum flux convergence (green), 10^{-5} m s^{-2} for the $8\Omega_e$ simulation. The reference time for this composition (lag 0 day) is the minimum in the Eady growth rate around each cycle (between two consecutive maxima of the mean zonal wind).

vertical shear of the zonal wind, which decreases the poleward bias in the Eady growth rate. In both regions, the increase of the mean zonal wind can further increase the baroclinicity and/or the eddy momentum flux convergence (as can be seen by the latter times in Figure 7). This growth occurs at the expense of these properties at equatorward latitudes, thus producing the poleward migration (Figure 1). This suggests that while the forcing of the migration of the jets at their flanks is due to the poleward bias of baroclinicity (due to the sphericity of the planet), at their cores, the eddy momentum flux convergences drive the migration. *Robinson* [2000] discussed the importance of the eddies in driving the poleward drift of both the mean zonal wind and the baroclinicity (as occurs at the jets' core in our simulations) through the equatorward propagation of momentum fluxes aloft (due to the sphericity of the planet). Thus, the sphericity of the planet plays an important role in affecting the poleward migration of the jets in both the flanks and the core of the jet.

In *Lee et al*. [2007], the migration of zonal wind anomalies starts in the tropics due to midlatitude wave breaking, while in our simulation the migration of the jets occurs only in the extratropics. However, the latter stages of their mechanism (the drift of zonal wind anomalies by eddy momentum flux convergence) are similar in both cases. In the extratropics, *Lorenz* [2014b] showed that the reflecting level is responsible for the poleward shift of the zonal wind anomalies, even when imposing a symmetric convergence of the vertical EP flux (i.e., no asymmetry in baroclinicity). This mechanism can also be suitable to explain the poleward biased eddy momentum flux convergence around the jet's core.

In steady state simulations, surface drag plays a major role as it balances the eddy momentum flux convergence [e.g., *James and Gray*, 1986; *Panetta*, 1993; *Robinson*, 1996, 2000; *Cai and Shin*, 2014, equation (1)]. However, as in *Lee et al*. [2007], we have found that systematically experimenting with variation of surface drag (by varying the surface roughness length) in these simulations (including cases where we significantly reduce the surface drag) has only a very minor affect on the jets and their migration (Figure 8). This is consistent with the fact that in equation (1) the leading order balance is between the zonal wind tendency and eddy momentum flux convergence. However, as we increase the surface friction beyond a certain value it begins to take an important role in the balance, and as a result, the migration rate decreases (Figure 8).

Furthermore, in the presented simulations both the divergence of the EP flux and measures of baroclinicity show a poleward bias around the jet's core (Figures 4, 5, and 6f), while the convergence of the EP flux occurs equatorward of the latitude of maximum baroclinic growth (Figure 7), as in *Robinson* [2000], and of the jet's position (Figure 3). However, the important role that friction plays (closing the mean meridional circulation in a steady state) in *Robinson*'s mechanism seems to be of secondary importance in these simulations (Figure 8).

5. The Properties of the Poleward Migration Over Multiple Rotation Rates

To demonstrate the robustness of the mechanism presented in section 4, we perform the same analysis for N_y, Eady growth rate, the supercriticality and their variables on representative model runs with different

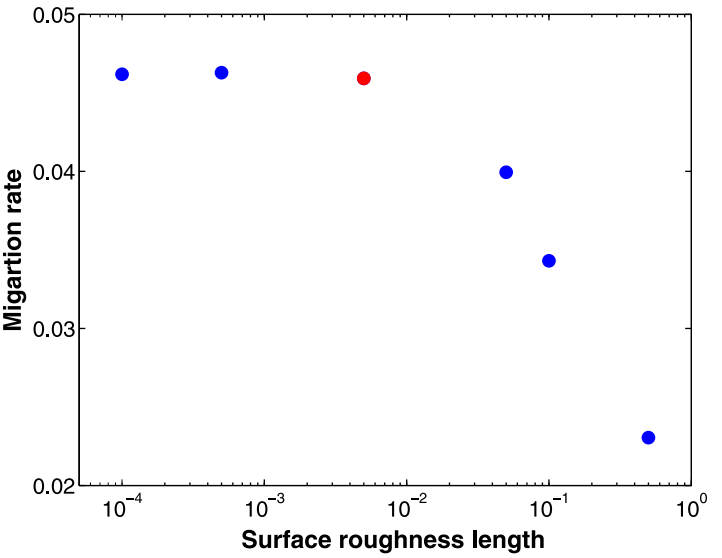

Figure 8. The migration rate, m s^{-1}, as a function of the surface roughness length, m. The red dot represents the value of surface friction used in the presented simulations.

rotation rates (6, 9, 12, and 16 Ω_e). The results are summarized in Table 1. The symmetry in U_z, S^2, and H around the jet's core is robust for all rotation rates, as the percentage of jets which experience a poleward bias is around 50%, and the ratio between the magnitude of the poleward bias and equatorward bias is around unity.

The poleward Coriolis bias within the jet width decreases with rotation rate (Figure 9 and Table 1). There are two competing mechanisms which affect the magnitude of the Coriolis parameter's poleward bias. On one hand, as the rotation rate increases, the Coriolis parameter grows more rapidly with latitude, which causes the poleward bias to increase. On the other hand, as the rotation rate increases the number of eddy-driven jets increases as well ($n_{\text{jet}} \propto \Omega^{0.81}$) due to the decrease in the eddy length scale (Figure 10), and therefore, the width of each one of the multiple baroclinic regions and the variation of the Coriolis parameter within each jet decreases. Since the number of jets increases with rotation rate, while the radius of the planet remains constant, the space between the jets decreases with rotation rate. Figure 11 shows the eddy-driven jet spacing as a function of latitude and rotation rate, where the jet spacing is defined as the length between two consecutive maxima of the zonal wind. The narrowing of the flanks causes the magnitude of the summed Coriolis parameter to decrease in both flanks, and thus to a total decrease in the magnitude of the poleward bias and resulting migration rate. The simulations show that the narrowing of the jets dominates the migration rate, over the increase in the value of the Coriolis parameter (Figure 1). The importance of the jet scaling on their meridional migration was also discussed by *Thompson* [2010] in the context of topographic variations.

The decrease in the poleward bias of the Coriolis parameter, leads also to a decrease in the poleward bias in the Eady growth rate and supercriticality (Figure 9 and Table 1). The mean net bias (Σ_p minus Σ_e) in Figure 12a demonstrates the effect of the jet narrowing on the poleward biased Eady growth rate and supercriticality with rotation rate. The poleward bias of N_y is robust in all the rotation rates (Figure 9 and Table 1), and also shows a decrease in the poleward bias of N_y as the rotation rate increases (Figure 9 and Table 1). Note that in Figure 9 even though the N_y bias ratio (red line) does not change with rotation rate, the actual bias value decreases, as consistent also with Figure 12b. Figure 12b also shows that the poleward bias of N_y is robust in all rotation rates (positive values) and that the mean net bias decreases with rotation rate, and is $\propto \Omega^{-1.2}$.

Based on our proposed mechanism for the poleward migration of the jets (section 4), the migration rate should be proportional to the net eddy momentum flux convergence, since this is the force that acts on the jets to propagate them poleward. Hence, we expect that the rate of migration should decrease with rotation rate as can be seen by comparing the slopes of the jet propagation with time in the Hovmoller plots in

Table 1. The Percentage of Jets Which Experienced a Poleward Bias, and the Magnitude of the Poleward Bias Relative to the Equatorward Bias for Each Property for Several Rotation Rate Simulations

Ω_e	U_z (s^{-1})	S^2 (s^{-2})	H (m)	f (s^{-1})	$f^2\beta^{-1}$ (m s^{-1})	σ (s^{-1})	ξ_c	N_y (m s^{-1})
6	53.38%, 0.97	71.30%, 1.10	52.59%, 0.99	97.12%, 1.32	99.95%, 1.71	90.48%, 1.22	100.00%, 1.78	90.68%, 1.46
9	55.90%, 0.99	55.84%, 1.07	47.93%, 0.97	86.81%, 1.25	99.67%, 1.54	80.65%, 1.21	99.93%, 1.77	87.26%, 1.45
12	55.61%, 0.99	53.00%, 1.07	42.23%, 0.97	79.96%, 1.21	98.15%, 1.42	76.10%, 1.21	98.53%, 1.70	86.99%, 1.45
16	58.37%, 1.00	56.72%, 1.06	43.08%, 0.95	73.20%, 1.18	78.40%, 1.37	72.51%, 1.20	87.57%, 1.71	86.38%, 1.46

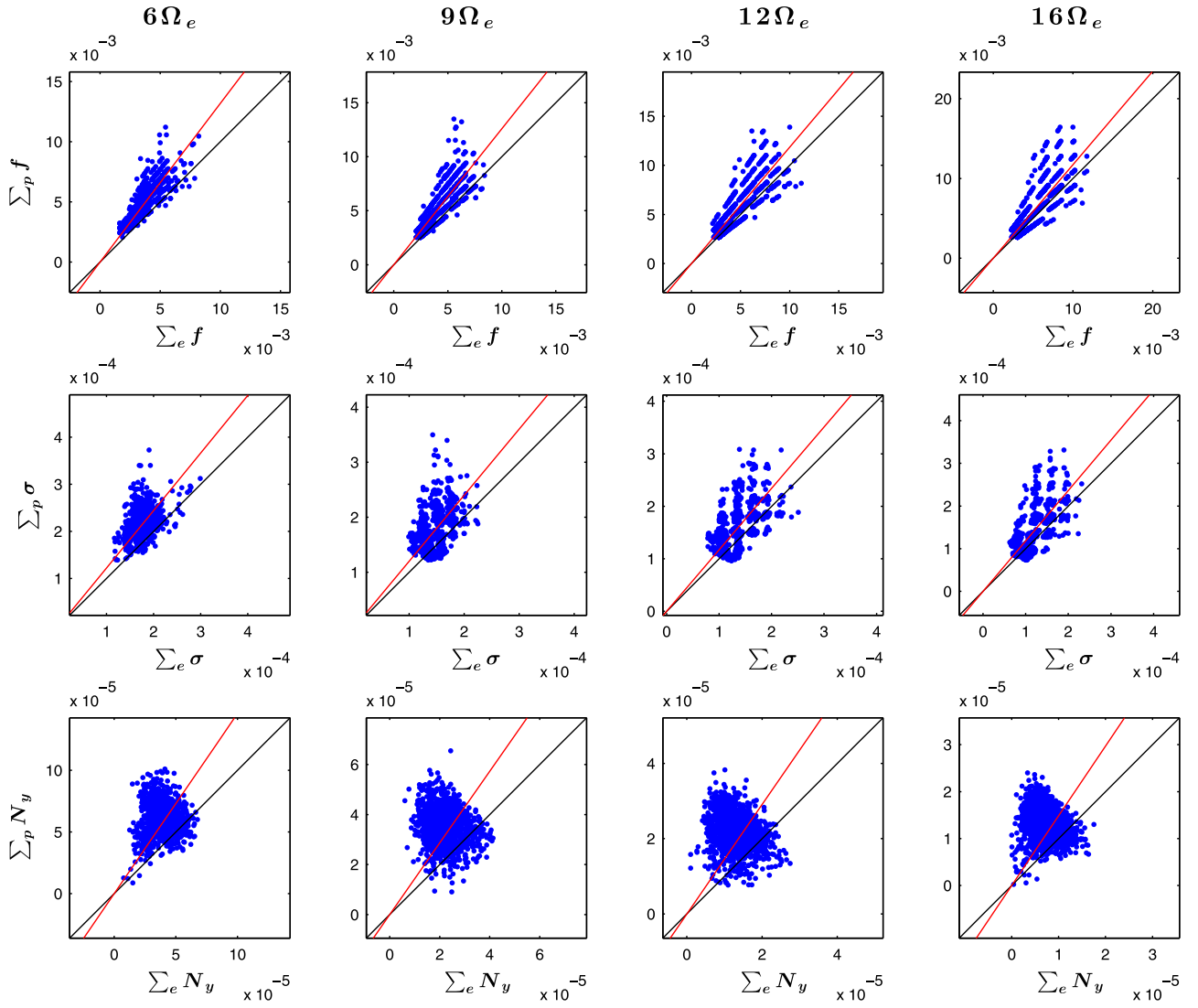

Figure 9. First, second, and third rows are the same as Figures 6c, 5a, and 4, respectively, only for 6 (first column), 9 (second column), 12 (third column), and 16 (fourth column) Ω_e runs. Bias values appear in Table 1.

Figure 1. *Feldstein* [1998] showed that in observations the poleward propagation speed decreases toward the midlatitude and increases toward the high latitudes. For the quantitative calculation of the migration rate (Figure 12c), we treat the meridional variations in the migration rate as a second-order process, and fit a linear trend over the entire baroclinic zone (from the subtropical jet to the latitude where the jets vanish) for all the jets in each rotation rate. Only simulations with a continuous migration were taken into account (simulations with a rotation rate larger than $5\Omega_e$). Figure 12c shows that the migration rate of the eddy-driven jets decreases with rotation rate and is $\propto \Omega^{-0.44}$. Figure 13, indeed, shows the nearly linear relation between the jet migration and the net eddy momentum flux convergence.

Nonetheless, due to the dependence of jet spacing on latitude as can be inferred from Figure 11, care should be taken when developing such scaling. In addition, unlike *Feldstein* [1998], in our simulations, the maximum propagation speed occurs at midlatitudes, although the meridional variations of the migration rate are small compared with its variations with rotation rate. The maximum propagation speed occurs at midlatitudes due to two reasons: First, as the jets propagate to higher latitudes the variations of the Coriolis parameter around their flanks (the beta effect) become smaller, which decrease the poleward bias of the baroclinic growth rate and N_y and thus the rate of migration. On the other hand, the jet spacing increases with latitude (Figure 11), thus, as explained previously for different rotation rates, at higher latitudes the

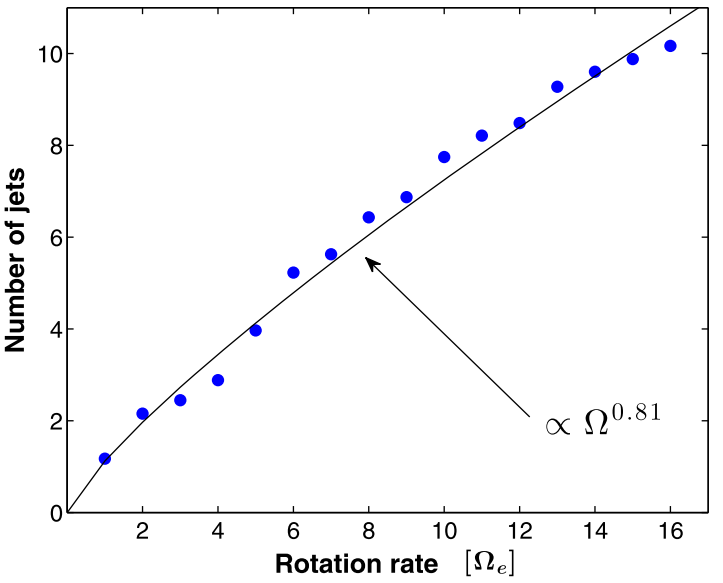

Figure 10. The average number of eddy-driven jets as a function of rotation rate.

wider jets can have a stronger poleward bias. As a result, the maximum propagation speed occurs at midlatitudes.

6. Discussion

In this study, we show using a high-resolution idealized moist GCM (the poleward migration of the eddy-driven jets does not depend on moisture processes, thus, repeating these simulations while eliminating the moisture effects gives the same results) that poleward migration of baroclinic eddy-driven jets can be generated due to an asymmetry in the eddy momentum flux convergence around the jet core. The larger eddy momentum flux convergence on the poleward flanks of the jets is consistent with an asymmetry in baroclinic growth around the jet's core. The type of bias (poleward or equatorward) in baroclinic growth, which we parameterize by the Eady growth rate and supercriticality, is determined by the ratio between the meridional change of the Coriolis parameter and the static stability (as the eddy-driven jets in our simulations are symmetric). In all simulations presented here the static stability is nearly symmetric around the jet's core. Hence, the Coriolis parameter is the main contributor to the poleward biased Eady growth rate and supercriticality. At the flanks of the jets, the baroclinic growth precedes the increase of the eddy momentum flux convergence, and thus drives the poleward migration of the jets due to the sphericity of the planet (the Coriolis parameter). On the other hand, around the jet's core, the eddy momentum flux convergence precedes the baroclinic growth. A possible mechanism for the latter was discussed by *Robinson* [2000], where the EP flux convergence (which occurs equatorward of their latitude of generation, due to the sphericity of the planet) shifts the baroclinicity and the mean zonal wind poleward, thorough a mean meridional circulation. Thus, the sphericity of the planet plays a major role in shifting the jet poleward [e.g., *Nakamura*, 1993; *Balasubramanian and Garner*, 1997; *Lorenz and Hartmann*, 2001; *Riviere*, 2009; *Thompson*, 2010]. *Son and Lee* [2006] showed that the meridional propagation of zonal anomalies is sensitive to the meridional temperature gradient forcing. Here, similarly, the vertical shear of the zonal wind times the Coriolis parameter (the meridional temperature gradient, using thermal wind balance) affects the properties of the migration. Beyond the possible application of this mechanism to the observed migrating anomalies in the extratropics [*Riehl et al.*, 1950; *Dickey et al.*, 1992; *Feldstein*, 1998], this

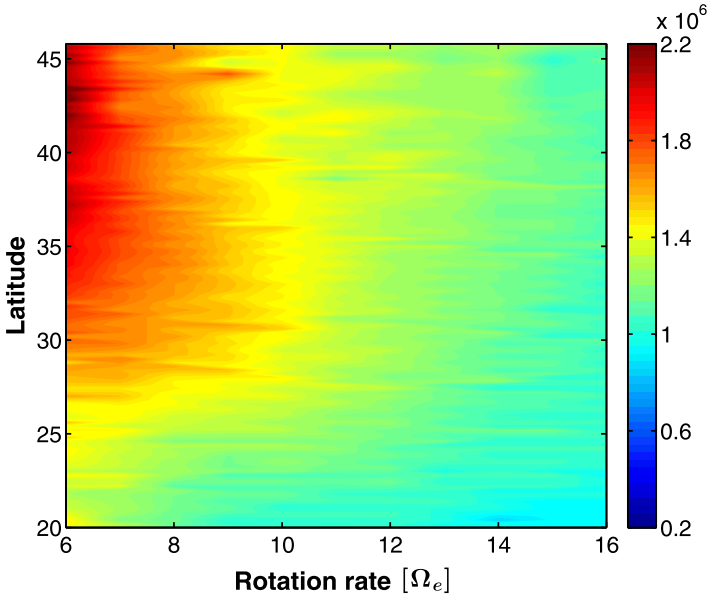

Figure 11. Jet spacing (m) as function of latitude and rotation rate.

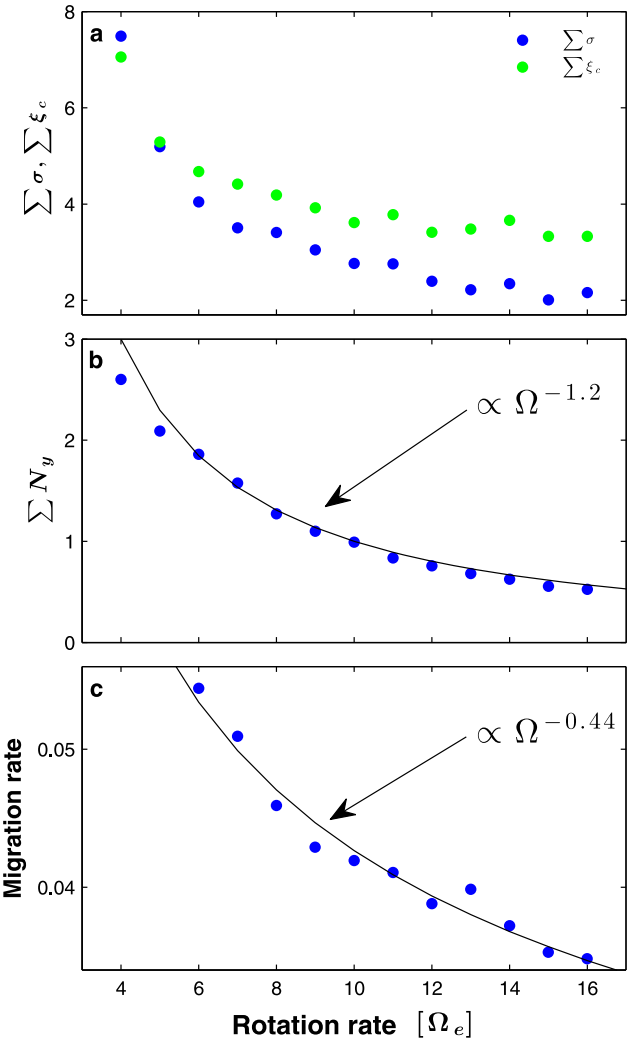

Figure 12. Dependence on rotation rate. (a) Net Eady growth rate (10^{-5} s^{-1}, blue) and the supercriticality parameter (green). Net refers to the sum of the Eady growth rate or supercriticality on the poleward flank minus the sum on the equatorward flank. (b) Net eddy momentum flux convergence (10^{-5} m s^{-2}, N_y). Net refers to the sum of the eddy momentum flux convergence on the poleward flank minus the sum on the equatorward flank. For the analysis of Figures 12a and 12b only simulations with a clear separation between the subtropical jet and the eddy-driven jets were taken into account ($\Omega > 3\Omega_e$). (c) Jet's migration rate (m s^{-1}). Only simulations with a continuous migration where taken into account for the analysis in Figure 12c ($\Omega > 5\Omega_e$).

work points to the general tendency of baroclinically driven jets to propagate meridionally with time.

The ratio between the Coriolis parameter and the static stability in the Eady growth rate and supercriticality, which plays a major role in determining the migration properties in this study and in *Chan et al.* [2007], also appears in the stretching term of the QG potential vorticity (QGPV). *Riviere* [2009] showed the effect that the absolute vorticity and stretching terms in the PV gradient have on the meridional location of the jet. While the absolute vorticity terms cause anticyclonic wave breaking and a poleward shift of the jet, the stretching term causes cyclonic wave breaking and an equatorward shift of the jet. The poleward biased Eady growth rate (Figures 5a and 9) implies that the Coriolis parameter causes a meridional asymmetry in the stretching term that leads to a meridional asymmetry in the shape of the jet, which may eventually cause a poleward migration. The supercriticality, however, contains the ratio between the stretching term and only the β term from the absolute vorticity. The poleward biased supercriticality (Figure 5b and Table 1) implies that both the stretching term and β may contribute to the poleward migration of the jets.

As discussed in section 1, it is difficult to test the jet migration mechanism on Earth using observational data. However, the regions of maximal momentum flux convergence on Earth have a strong correlation to the strongly baroclinic regions, and baroclinically generated cyclones on average do migrate poleward downstream of their source regions [*Coronel et al.*, 2015]. This phenomenon is particularly evident in the Atlantic and Pacific storm track regions [*Orlanski*, 1998; *Riviere*, 2009; *Kaspi and Schneider*, 2013], and it is possible that the poleward migration of zonal anomalies is also related to this spatial poleward tilt.

Lee [2005] used the Rhines scale and the supercriticality from *Phillips* [1956] in order to state that the number of eddy-driven jets is $n_{\text{jet}} \propto \left(\frac{a}{\Theta_m}\right)^{0.5}$, where a is the planet radius and Θ_m is half of the potential temperature difference between the equator to pole. Lee's model suggests that the number of eddy-driven jets should be $\propto \Omega^{0.5}$. Figure 10 shows that in our simulations, the number of eddy-driven jets is $n_{\text{jet}} \propto \Omega^{0.81}$, and by including the subtropical jet, $n_{\text{jet}} \propto \Omega^{0.52}$. Since in these simulations, the jet scaling follows the Rhines scale [*Chemke and Kaspi*, 2015], and in *Lee* [2005] the width of the baroclinic zone was taken to be constant, the above discrepancy could be explained by the variations of the width of the baroclinic zone with rotation rate.

O'Gorman and Schneider [2008b] showed that the meridional jet spacing approximately matches the eddy length, which does not vary much with latitude, and the Rhines scale. This coincides with our finding

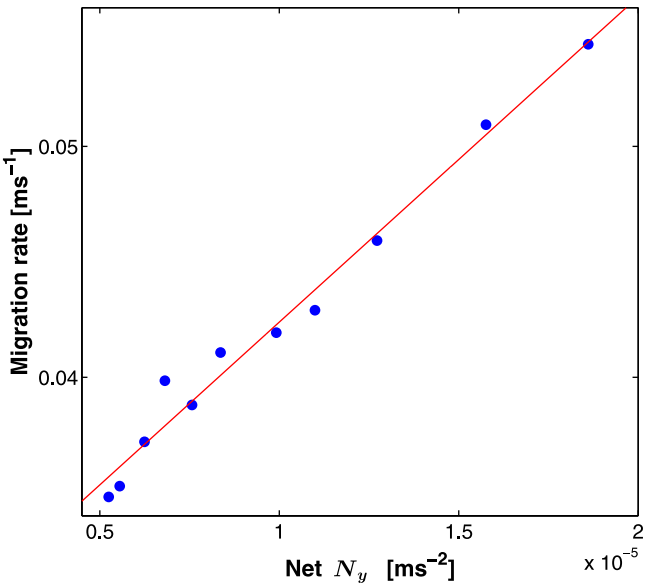

Figure 13. Jet migration rate as a function of net eddy momentum flux convergence for different rotation rates. Net refers to the sum of the eddy momentum flux convergence on the poleward flank minus the sum on the equatorward flank. The red line is a linear fit, and has a slope of 1.4×10^3.

regarding the dependence of the jet space on rotation rate (Figure 11). However, our results do show that the space between the jets increases with latitude, as was pointed out by *Huang and Robinson* [1998], and this increase becomes more moderate at higher rotation rates (Figure 11). We further discuss the properties of the jet spacing on a multiple jet planet in *Chemke and Kaspi* [2015].

Williams [2003] showed that an equatorward migration of eddy-driven jets can occur in a Jupiter parameter regime, due to an asymmetry in the eddy momentum fluxes, which are larger on the equatorward side of the jets. Following on the mechanism presented here, such a case may exist if the static stability on Jupiter increases poleward faster than the Coriolis parameter. However, all wind and thermal structure data for Jupiter are limited to the outer cloud level, and therefore currently we have no estimates for the static stability, nor do we know the depth to which the dynamic weather layer may extend [*Kaspi*, 2013]. If indeed the observed jets on Jupiter are mainly eddy driven [*Salyk et al*., 2006], then Jupiter lies in the regime where such poleward migration is possible, however current detailed wind observations, which all rely on cloud tracking have been interpolated only for very specific and short times during spacecraft flybys [e.g., *Choi and Showman*, 2011].

Acknowledgments
We thank Janni Yuval and Nili Harnik for very fruitful discussions during the preparation of this paper and Eli Tziperman, Eli Galanti, Talia Tamarin, Hila Afargan, and the reviewers for their comments on this paper. This research has been supported by an EU-FP7 Marie Curie Career Integration grant (CIG-304202), the Israeli Science Foundation (grants 1310/12 and 1859/12), the German-Israeli Foundation for Scientific Research and Development (grant 2300-2295.14/2011), and the Feinberg Graduate School at the Weizmann Institute of Science. All the data presented in this paper can be provided upon request at rei.chemke@weizmann.ac.il.

References

Balasubramanian, G., and S. T. Garner (1997), The role of momentum fluxes in shaping the life cycle of a baroclinic wave, *J. Atmos. Sci.*, *54*(4), 510–533.
Barnes, E. A., and D. W. Thompson (2014), Comparing the roles of barotropic versus baroclinic feedbacks in the atmosphere's response to mechanical forcing, *J. Atmos. Sci.*, *71*(1), 177–194.
Blackmon, M. L. (1976), A climatological spectral study of the 500 mb geopotential height of the northern hemisphere, *J. Atmos. Sci.*, *33*(8), 1607–1623.
Blackmon, M. L., J. M. Wallace, N. Lau, and S. L. Mullen (1977), An observational study of the northern hemisphere wintertime circulation, *J. Atmos. Sci.*, *34*(7), 1040–1053.
Cai, M., and C. S. Shin (2014), Total flow perspective of atmospheric mass and angular momentum circulations: Boreal winter mean state, *J. Atmos. Sci.*, *71*(6), 2244–2263.
Chan, C. J., R. A. Plumb, and I. Cerovecki (2007), Annular modes in a multiple migrating zonal jet regime, *J. Atmos. Sci.*, *64*(11), 4053–4068.
Chang, E. K. M., S. Lee, and K. L. Swanson (2002), Storm track dynamics, *J. Clim.*, *15*, 2163–2183.
Charney, J. G. (1947), The dynamics of long waves in a baroclinic westerly current, *J. Meteorol.*, *4*(5), 136–162.
Chemke, R., and Y. Kaspi (2015), The latitudinal dependence of atmospheric jet scales and macroturbulent energy cascades, *J. Atmos. Sci.*, in press.
Cho, J., and L. M. Polvani (1996), The formation of jets and vortices from freely-evolving shallow water turbulence on the surface of a sphere, *Phys. Fluids*, *8*, 1531–1552.
Choi, D. S., and A. P. Showman (2011), Power spectral analysis of Jupiter's clouds and kinetic energy from Cassini, *Icarus*, *216*(2), 597–609.
Coronel, B., D. Ricard, G. Rivire, and P. Arbogast (2015), Role of moist processes in the tracks of idealized mid-latitude surface cyclones, *J. Atmos. Sci.*, *72*(8), 2979–2996.
Dickey, J. O., S. L. Marcus, and R. Hide (1992), Global propagation of interannual fluctuations in atmospheric angular momentum, *Nature*, *357*(6378), 484–488.
Eady, E. T. (1949), Long waves and cyclonic waves, *Tellus*, *1*(3), 33–52.
Edmon, J. H. J., B. J. Hoskins, and M. E. McIntyre (1980), Eliassen-Palm cross sections for the troposphere, *J. Atmos. Sci.*, *37*(12), 2600–2612.
Feldstein, S. B. (1998), An observational study of the intraseasonal poleward propagation of zonal mean flow anomalies, *J. Atmos. Sci.*, *55*(15), 2516–2529.
Frierson, D. M. W., I. M. Held, and P. Zurita-Gotor (2006), A gray-radiation aquaplanet moist GCM. Part I: Static stability and eddy scale, *J. Atmos. Sci.*, *63*(10), 2548–2566.
Held, I. M. (1982), On the height of the tropopause and the static stability of the troposphere, *J. Atmos. Sci.*, *39*(2), 412–417.
Held, I. M., and B. J. Hoskins (1985), Large-scale eddies and the general circulation of the troposphere, *Adv. Geophys.*, *28*, 3–31.
Held, I. M., and A. Y. Hou (1980), Nonlinear axially symmetric circulations in a nearly in viscid atmosphere, *J. Atmos. Sci.*, *37*, 515–533.

Held, I. M., and V. D. Larichev (1996), A scaling theory for horizontally homogeneous, baroclinically unstable flow on a beta plane, *J. Atmos. Sci.*, *53*(7), 946–952.
Hoskins, B. J., and P. J. Valdes (1990), On the existence of storm-tracks, *J. Atmos. Sci.*, *47*, 1854–1864.
Hoskins, B. J., I. N. James, and G. H. White (1983), The shape, propagation and mean-flow interaction of large-scale weather systems, *J. Atmos. Sci.*, *40*(7), 1595–1612.
Huang, H. P., and W. A. Robinson (1998), Two-dimensional turbulence and persistent jets in a global barotropic model, *J. Atmos. Sci.*, *55*(4), 611–632.
Ioannou, P., and R. S. Lindzen (1986), Baroclinic instability in the presence of barotropic jets, *J. Atmos. Sci.*, *43*(2), 2999–3014.
James, I. N., and J. P. Dodd (1996), A mechanism for the low frequency variability of the mid latitude troposphere, *Q. J. R. Meteorol. Soc.*, *122*(533), 1197–1210.
James, I. N., and L. J. Gray (1986), Concerning the effect of surface drag on the circulation of a baroclinic planetary atmosphere, *Q. J. R. Meteorol. Soc.*, *112*(474), 1231–1250.
James, P. M., K. Fraedrich, and I. N. James (1994), Wave zonal flow interaction and ultra low frequency variability in a simplified global circulation model, *Q. J. R. Meteorol. Soc.*, *120*(518), 1045–1067.
Kaspi, Y. (2013), Inferring the depth of the zonal jets on Jupiter and Saturn from odd gravity harmonics, *Geophys. Res. Lett.*, *40*, 676–680, doi:10.1029/2012GL053873.
Kaspi, Y., and T. Schneider (2011), Downstream self-destruction of storm tracks, *J. Atmos. Sci.*, *68*, 2459–2464.
Kaspi, Y., and T. Schneider (2013), The role of stationary eddies in shaping midlatitude storm tracks, *J. Atmos. Sci.*, *70*, 2596–2613.
Kaspi, Y., and A. P. Showman (2015), Three dimensional atmospheric dynamics of terrestial exoplanets over a wide range of orbital and atmospheric parameters, *Astrophys. J.*, *804*, 60, doi:10.1088/0004-637X/804/1/60.
Kidston, J., G. K. Vallis, S. M. Dean, and J. A. Renwick (2011), Can the increase in the eddy length scale under global warming cause the poleward shift of the jet streams?, *J. Clim.*, *24*(14), 3764–3780.
Lee, S. (2005), Baroclinic multiple zonal jets on the sphere, *J. Atmos. Sci.*, *62*(7), 2482–2498.
Lee, S., S. W. Son, K. Grise, and S. B. Feldstein (2007), A mechanism for the poleward propagation of zonal mean flow anomalies, *J. Atmos. Sci.*, *64*(3), 849–868.
Lindzen, R. S., and B. Farrell (1980), A simple approximate result for the maximum growth rate of baroclinic instabilities, *J. Atmos. Sci.*, *37*(7), 1648–1654.
Lorenz, D. J. (2014a), Understanding mid-latitude jet variability and change using Rossby wave chromatography: Poleward shifted jets in response to external forcing, *J. Atmos. Sci.*, *71*, 2370–2389.
Lorenz, D. J. (2014b), Understanding midlatitude jet variability and change using Rossby wave chromatography: Wave-mean flow interaction, *J. Atmos. Sci.*, *71*(10), 3684–3705.
Lorenz, D. J., and D. L. Hartmann (2001), Eddy-zonal flow feedback in the southern hemisphere, *J. Atmos. Sci.*, *58*(21), 3312–3327.
Lorenz, E. N. (1955), Available potential energy and the maintenance of the general circulation, *Tellus*, *7*(2), 157–167.
Merlis, T. M., and T. Schneider (2009), Scales of linear baroclinic instability and macroturbulence in dry atmospheres, *J. Atmos. Sci.*, *66*(6), 1821–1833.
Mitchell, J. L., and G. K. Vallis (2010), The transition to superrotation in terrestrial atmospheres, *J. Geophys. Res.*, *115*, E12008, doi:10.1029/2010JE003587.
Nakamura, N. (1993), Momentum flux, flow symmetry, and the nonlinear barotropic governor, *J. Atmos. Sci.*, *50*(14), 2159–2179.
Navarra, A., and G. Boccaletti (2002), Numerical general circulation experiments of sensitivity to earth rotation rate, *Clim. Dyn.*, *19*(5–6), 467–483.
O'Gorman, P. A., and T. Schneider (2008a), The hydrological cycle over a wide range of climates simulated with an idealized GCM, *J. Clim.*, *21*(15), 3815–3832.
O'Gorman, P. A., and T. Schneider (2008b), Weather-layer dynamics of baroclinic eddies and multiple jets in an idealized general circulation model, *J. Atmos. Sci.*, *65*(2), 524–535.
Orlanski, I. (1998), Poleward deflection of storm tracks, *J. Atmos. Sci.*, *55*, 2577–2602.
Orlanski, I. (2003), Bifurcation in eddy life cycles: Implications for storm track variability, *J. Atmos. Sci.*, *60*(8), 993–1023.
Panetta, R. L. (1993), Zonal jets in wide baroclinically unstable regions: Persistence and scale selection, *J. Atmos. Sci.*, *50*(14), 2073–2106.
Pedlosky, J. (1987), *Geophysical Fluid Dynamics*, Springer-Verlag, N. Y.
Phillips, N. A. (1954), Energy transformations and meridional circulations associated with simple baroclinic waves in a two level quasi-geostrophic model, *Tellus*, *6*(3), 273–286.
Phillips, N. A. (1956), The general circulation of the atmosphere: A numerical experiment, *Q. J. R. Meteorol. Soc.*, *82*(352), 123–164.
Riehl, H., T. C. Yeh, and N. E. La Seur (1950), A study of variations of the general circulation, *J. Meteorol.*, *7*(3), 181–194.
Riviere, G. (2009), Effect of latitudinal variations in low level baroclinicity on eddy life cycles and upper tropospheric wave breaking processes, *J. Atmos. Sci.*, *66*(6), 1569–1592.
Robinson, W. A. (1996), Does eddy feedback sustain variability in the zonal index?, *J. Atmos. Sci.*, *53*(23), 3556–3569.
Robinson, W. A. (2000), A baroclinic mechanism for the eddy feedback on the zonal index, *J. Atmos. Sci.*, *57*(3), 415–422.
Salyk, C., A. P. Ingersoll, J. Lorre, A. Vasavada, and A. D. Del Genio (2006), Interaction between eddies and mean flow in Jupiter's atmosphere: Analysis of Cassini imaging data, *Icarus*, *185*, 430–442.
Schneider, T., and C. C. Walker (2008), Scaling laws and regime transitions of macroturbulence in dry atmospheres, *J. Atmos. Sci.*, *65*, 2153–2173.
Simmons, A. J., and B. J. Hoskins (1978), The life cycles of some nonlinear baroclinic waves, *J. Atmos. Sci.*, *35*(3), 414–432.
Smith, K. S. (2007), The geography of linear baroclinic instability in Earth's oceans, *J. Mar. Res.*, *65*(5), 655–683.
Son, S.-W., and S. Lee (2006), Preferred modes of variability and their relationship with climate change, *J. Clim.*, *19*(10), 2063–2075.
Stone, P. H. (1966), On non-geostrophic baroclinic stability, *J. Atmos. Sci.*, *23*(4), 390–400.
Thompson, A. F. (2010), Jet formation and evolution in baroclinic turbulence with simple topography, *J. Phys. Oceanogr.*, *40*(2), 257–278.
Vallis, G. K. (2006), *Atmospheric and Oceanic Fluid Dynamics*, 770 pp., Cambridge Univ. Press, Cambridge, U. K.
Vallis, G. K., and M. E. Maltrud (1993), Generation of mean flows and jets on a beta plane and over topography, *J. Phys. Oceanogr.*, *23*(7), 1346–1362.
Walker, C. C., and T. Schneider (2006), Eddy influences on Hadley circulations: Simulations with an idealized GCM, *J. Atmos. Sci.*, *63*, 3333–3350.
Whitaker, J. S., and C. Snyder (1993), The effects of spherical geometry on the evolution of baroclinic waves, *J. Atmos. Sci.*, *50*(4), 597–612.
Williams, G. P. (2003), Jovian dynamics. Part III: Multiple, migrating, and equatorial jets, *J. Atmos. Sci.*, *60*(10), 1270–1296.
Williams, G. P., and J. L. Holloway (1982), The range and unity of planetary circulations, *Nature*, *297*(5864), 295–299.
Zurita-Gotor, P., J. Blanco-Fuentes, and E. P. Gerber (2014), The impact of baroclinic eddy feedback on the persistence of jet variability in the two-layer model, *J. Atmos. Sci.*, *71*(1), 410–429.